

Magnetic field-induced squeezing effect at RHIC and at the LHC

Long-Gang Pang,¹ Gergely Endrődi,^{2,3} and Hannah Petersen^{1,3,4}

¹Frankfurt Institute for Advanced Studies, Ruth-Moufang-Strasse 1, 60438 Frankfurt am Main, Germany

²Institute for Theoretical Physics, University Regensburg, D-93040 Regensburg, Germany

³Institute for Theoretical Physics, Goethe University,

Max-von-Laue-Strasse 1, 60438 Frankfurt am Main, Germany

⁴GSI Helmholtzzentrum für Schwerionenforschung, Planckstr. 1, 64291 Darmstadt, Germany

In off-central heavy-ion collisions, the quark-gluon plasma (QGP) is exposed to the strongest magnetic fields ever created in the universe. Due to the paramagnetic nature of the QGP at high temperatures, the spatially inhomogeneous magnetic field configuration exerts an anisotropic force density that competes with the pressure gradients resulting from purely geometric effects. In this paper, we simulate (3+1)-dimensional ideal hydrodynamics with external magnetic fields to estimate the effect of this force density on the anisotropic expansion of the QGP in collisions at RHIC and at the LHC. While negligible for quickly decaying magnetic fields, we find that long-lived fields generate a substantial force density that suppresses the momentum anisotropy of the plasma by up to 20% at the LHC energy, and also leaves its imprint on the elliptic flow v_2 of charged pions.

PACS numbers: 12.38.Mh, 25.75.Ld, 25.75.Gz

I. INTRODUCTION

One of the most striking phenomena in high-energy heavy-ion collisions is the strong collective flow of the hot quark-gluon plasma (QGP), caused by the relativistic hydrodynamic expansion driven by local pressure gradients. For off-central collisions, the anisotropy of the initial geometry enhances this collective flow in the reaction plane and leads to a non-vanishing elliptic flow v_2 of charged hadrons observed in the experiment. An additional relevant feature of such collisions is the generation of extremely strong magnetic fields [1–5] created by the colliding charged beams moving at relativistic speed. The impact of these fields in heavy-ion collisions was first explored in relation with the chiral magnetic effect [6, 7]. Later studies also discussed the role of magnetic fields on jet energy loss [8], on the thermal photon and di-lepton production rate [9, 10] and on the collective expansion of the fireball [11, 12].

In this paper we concentrate on the response of the QGP to the magnetic field in terms of the induced magnetization,

$$\mathbf{M} \equiv -\frac{\partial f}{\partial \mathbf{B}}, \quad (1)$$

where f is the free energy density of the thermodynamic system. Lattice QCD calculations have demonstrated that in the range of magnetic fields and temperatures relevant for heavy-ion collisions $\mathbf{M} \parallel \mathbf{B}$, that is to say, the QGP behaves as a paramagnet¹ [15–20]. It is well known that, if exposed to inhomogeneous magnetic fields, paramagnetic materials move along the gradient of $|\mathbf{B}|$ – as opposed to diamagnets that move in the opposite

direction [21]. Based on model descriptions of heavy-ion collisions (see below), off-central events are expected to exhibit inhomogeneous fields with a strong spatial anisotropy. As Ref. [12] pointed out, such a magnetic field configuration exerts an anisotropic force density on the QGP that compresses matter in the transverse plane. This force density – dubbed *paramagnetic squeezing* – arises as the system minimizes its free energy and reads

$$\mathbf{F} \equiv -\nabla f = (\nabla \mathbf{B}) \cdot \mathbf{M}. \quad (2)$$

It was recognized that the squeezing force density might affect the collective expansion and, eventually, have an impact on the elliptic flow v_2 of the final charged hadrons. A first estimate of this effect was made by comparing the magnitudes of the squeezing force density with those of the pressure gradients at initial time for RHIC and LHC energies [12], revealing that the effect might be marginal for RHIC but substantial for LHC collisions.

In this paper we improve on this simplistic estimate in various aspects. We simulate (3+1)-dimensional ideal hydrodynamics to determine the time-evolution of the energy density and the fluid velocity in the presence of an external magnetic field profile. This profile is assumed to be given in terms of a few parameters that control the magnitude, the spatial distribution and the time-evolution of the magnetic field. Systematically varying these parameters enables us to study the influence of paramagnetic squeezing in different limits. The effect of the squeezing force density is taken into account throughout the hydrodynamic expansion to determine the impact on momentum anisotropy and to calculate the time integrated effect on v_2 of charged particles on the freeze out hypersurface.

Note that in this setup we treat the magnetic field as an external degree of freedom, i.e., we neglect the back-reaction of the fluid on \mathbf{B} . A fully consistent description of the entangled evolution of the hydrodynamic expansion and of the electromagnetic field would require (3+1)-

¹ Previously, the paramagnetic response was also predicted in perturbation theory [13] and in the hadron resonance gas model [14].

dimensional relativistic magnetohydrodynamics, which, however, is still under development [22, 23]. We further mention that magnetic field-induced effects on the fluid expansion have also been discussed in terms of a comparison of the magnetic and fluid energy densities [11, 24] and of the one-dimensional longitudinal boost-invariant Bjorken flow [25, 26].

The rest of this paper is organized as follows. In Sec. II we introduce the (3+1)-dimensional ideal hydrodynamic model and the parameters used for the magnetic field and the hydrodynamic expansions. The relative magnitude of the squeezing force density and the initial pressure gradients, together with the effect of the squeezing on the fluid expansion and on the elliptic flow of final charged hadrons are shown in Sec. III both for Pb+Pb $\sqrt{s_{NN}} = 2.76$ TeV collisions and for Au+Au $\sqrt{s_{NN}} = 200$ GeV collisions. This is followed by Sec. IV, which summarizes the results and presents a short outlook.

II. SETUP AND METHODS

We use (3+1)-dimensional ideal hydrodynamic simulations [27, 28], as implemented in the CLVisc code parallelized on GPUs using OpenCL [28]. For simplicity, no viscous corrections are taken into account in the current study.

Hydrodynamic equations

The hydrodynamic equations in the presence of the squeezing force (2) read [29]

$$\partial_\mu T^{\mu\nu} = F^\nu, \quad (3)$$

where $T^{\mu\nu} = (\varepsilon + P)u^\mu u^\nu - Pg^{\mu\nu}$ is the energy momentum tensor for ideal hydrodynamics, $u^\mu = \gamma(1, \mathbf{v})$ denotes the fluid velocity four vector, ε the energy density and P the pressure². The latter is given as a function of ε by the equation of state (EoS). The lattice QCD equation of state from the Wuppertal-Budapest group (2014) [30] is used in the current study. The space-time coordinate axes are x (impact parameter direction), y (direction perpendicular to the reaction plane), η_s (space-time rapidity) and τ (proper time).

According to lattice QCD calculations [12, 20], the leading expansion for the magnetization – $\mathbf{M} = \chi \mathbf{B}$ in terms of the magnetic susceptibility χ – is a reasonable

approximation for the range of magnetic fields and temperatures we are interested in. Using the susceptibility, the squeezing force density F^ν on the right hand side of Eq. (3) reads

$$F^x = \frac{\chi}{2} \partial_x |\mathbf{B}|^2, \quad F^y = \frac{\chi}{2} \partial_y |\mathbf{B}|^2, \quad F^\tau = F^{\eta_s} = 0. \quad (4)$$

Here we assumed that the dynamics relevant for the anisotropic flow is governed by forces in the transverse plane and, accordingly, set the longitudinal force to zero. This choice may also be thought of as a setup where the magnetic field is constant in the longitudinal direction within the QGP. In addition, we have checked that enforcing zero energy input $u_\mu F^\mu = 0$ from the force (as expected in a purely magnetic background) by setting the zero component F^τ to $v_x F^x + v_y F^y$ changes the momentum anisotropy by only $\sim 1\%$ and can thus be neglected.

The most up-to-date lattice QCD results for the magnetic susceptibility can be found in Ref. [20]. A simple parameterization that agrees with the data within two standard deviations above $T = 110$ MeV and matches perturbation theory at high temperatures (cf. Ref. [20]) is

$$T > 110 \text{ MeV}: \quad \chi(T) = \frac{e^2}{3\pi^2} \log \frac{T}{110 \text{ MeV}}, \quad (5)$$

where e denotes the elementary charge. Below it will be convenient to give the magnetic field in terms of e , since the combination eB has units GeV^2 . Notice that we use isothermal freezeout conditions, where the hypersurface is determined by a constant temperature $T = 137$ MeV.

Magnetic field profile

In order to calculate F^ν , knowledge of the spatial profile of the magnetic field is necessary at each point in time. As it turns out, the largest uncertainty in this description is the time-dependence $\mathbf{B}(\tau)$. While the magnetic field due to the spectators would drop very quickly in the vacuum [6] (in fact, by a few orders of magnitude within 1 fm/c), it has been speculated that the field could survive much longer in the QGP if the electrical conductivity of the plasma is high [10, 31, 32]. In the pre-equilibrium stage, the decay of the magnetic field might also be delayed by charged quark-antiquark pairs due to gluon splitting and the Schwinger mechanism [33], see also Ref. [10]. In this paper, the terms ‘medium’ and ‘vacuum’ are used to denote a collision system with or without electrical conductivity.

Although the evolution of the magnetic field is likely to be affected considerably by the medium, the dependence of B on the collision parameters can be estimated by using the Lienard-Wiechert potential of the colliding nucleons in the vacuum. While the magnetic field was found [1] to depend rather weakly on the electric charge number Z of the nuclei ($B \propto Z^{1/3}$), it was observed to be strongly influenced by the impact parameter b and

² Notice that the energy-momentum tensor of the magnetic field – i.e., terms like $\mathbf{B}^2/2$ in the energy density – are not taken into account here. This is due to the fact that the field is considered external so that, for example, its energy density is independent of the fluid dynamics. The only effect appears due to the interaction of \mathbf{B} with the fluid through the magnetization.

the collision beam energy $\sqrt{s_{NN}}$ [3, 4, 6]. The spatial distribution of the magnetic field in the reaction plane was studied both in a setting with uniform nucleon density in the nucleus [34] as well as a more realistic Woods-Saxon nucleon density distribution [4, 35], showing a pronounced anisotropy in the magnetic field profile – namely a steep fall-off along the impact parameter direction and a slower variation perpendicular to the reaction plane.

Based on these considerations, the transverse distribution of a longitudinal boost invariant – i.e., η_s -independent – magnetic field is parameterized as,

$$eB(x, y, \tau) = eB_0 \exp\left(-\frac{x^2}{2\sigma_x^2} - \frac{y^2}{2\sigma_y^2}\right) \exp\left(-\frac{\tau}{t_d}\right), \quad (6)$$

where eB_0 is the amplitude of the magnetic field, which is taken to be 0.09 GeV^2 ($\approx 5 m_\pi^2$) for RHIC energy and 1.33 GeV^2 ($\approx 70 m_\pi^2$) for LHC energy [4] while σ_x and σ_y are the Gaussian widths along the x and y directions, respectively. Since the time evolution of the magnetic field in the pre-equilibrium stage is still unknown, we use an exponential decay for this, with a lifetime t_d varying between 0.1 fm and 1.9 fm. The various different settings used in the paper are summarized in Table. I.

setting	eB_0 [GeV ²]	t_d [fm]	σ_x [fm]	σ_y [fm]
A	0.09	1.9	1.3	2.6
B	1.33	0.1	1.3	2.6
C	1.33	0.5	1.3	2.6
D	1.33	1.0	1.3	2.6
E	1.33	1.9	1.3	2.6
F	1.33	1.9	2.4	4.8
G	1.0	1.9	2.4	4.8

Table I: The configurations for the space-time profile of the magnetic field, inspired by previous studies of magnetic fields in the vacuum [6, 35] and in the QGP [10, 31, 34, 36–40] (settings A–G) together with the reference configuration at $eB = 0$.

Four different parameters for the lifetime $0.1 \text{ fm} \leq t_d \leq 1.9 \text{ fm}$ are used for Pb+Pb collision to get the spatial distribution of the squeezing force density during the hydrodynamic evolution (which starts at the thermalization time τ_0). As shown in Fig. 1, the maximum force density at time $\tau_0 = 0.2 \text{ fm}$ is in the range $(2 \dots 4) \text{ GeV/fm}^4$ for long-lived fields, whereas it is merely 0.08 GeV/fm^4 for $t_d = 0.1 \text{ fm}$.

Initial state and thermalization time

The initial energy density distribution is given by the optical Glauber model,

$$\varepsilon(\tau_0, x, y, \eta_s) = K \cdot (0.95N_{wn} + 0.05N_{bc}) \times \exp\left[-\frac{(|\eta_s| - \eta_w/2)^2}{2\sigma_\eta^2}\right] \Theta(|\eta_s| - \eta_w/2), \quad (7)$$

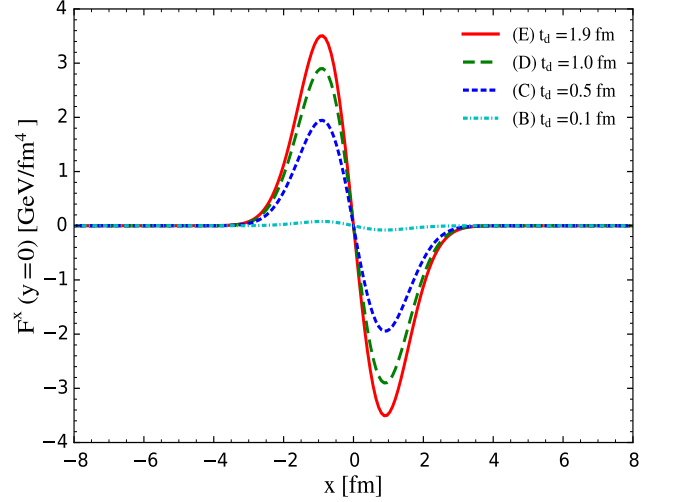


Figure 1: The squeezing force density (F^x) along the x axis at $\tau_0 = 0.2 \text{ fm}$ with the magnetic field given by settings (B) $t_d = 0.1 \text{ fm}$, (C) $t_d = 0.5 \text{ fm}$, (D) $t_d = 1.0 \text{ fm}$ and (E) $t_d = 1.9 \text{ fm}$, for Pb+Pb $\sqrt{s_{NN}} = 2.76 \text{ TeV}$ collisions with local temperature from (3+1)D hydrodynamics.

where a large fraction of the initial energy deposition is assumed to come from the soft part that is proportional to $0.95N_{wn}$ (N_{wn} is the number of wounded nucleons), and a smaller fraction is proportional to $0.05N_{bc}$ (N_{bc} is the number of binary collisions). In calculating N_{wn} and N_{bc} , the inelastic scattering cross sections σ_0 are set to 64 mb for Pb+Pb 2.76 TeV and 40 mb for Au+Au 200 GeV collisions. One envelope distribution is used along the longitudinal direction, where the width of the plateau η_w at mid-rapidity and the width of the fast fall-off σ_η at large rapidity are set to 5.9 and 0.4 for Au+Au $\sqrt{s_{NN}} = 200 \text{ GeV}$ and 7.0 and 0.6 for Pb+Pb $\sqrt{s_{NN}} = 2.76 \text{ TeV}$ collisions. The parameter K is fixed by the maximum energy density ε_0 given in Table. III, for most central collisions at RHIC and LHC energy.

In the optical Glauber model, the nucleon densities of the Pb and Au nucleus are described by the Woods-Saxon distribution,

$$\rho(r) = \frac{\rho_0}{\exp\left(\frac{r-R}{d}\right) + 1}, \quad (8)$$

where R is the radius of the nucleus, ρ_0 is the average nucleon density and d is the diffusiveness. The parameters used in the optical Glauber model are listed in Table. II,

nucleus	A	ρ_0 [1/fm ³]	R [fm]	d [fm]
Pb	208	0.17	6.38	0.535
Au	197	0.17	6.62	0.546

Table II: Parameters used in the Woods-Saxon distribution for Pb and Au nucleus.

The effect of the squeezing force (with small t_d) is sensitive to the strength of the magnetic field at initial thermalization time τ_0 . According to the analytical solution of 1D Bjorken hydrodynamics

$$\varepsilon/\varepsilon_0 = (\tau_0/\tau)^{1+c_s^2}, \quad s/s_0 = (\varepsilon/\varepsilon_0)^{1/(1+c_s^2)},$$

where $\varepsilon(\varepsilon_0)$ and $s(s_0)$ are the energy density and entropy density at $\tau(\tau_0)$ respectively and c_s is the speed of sound. Therefore, in this approximation the evolution $s(\tau)$ is invariant under changes of τ_0 as long as the combination $\tau_0 s_0$ is kept constant. (The entropy density at τ_0 is obtained from the EoS and the maximum energy density ε_0 .) As shown in Table. III, three groups of initial thermalization time τ_0 and maximum energy density ε_0 are listed that give the same charged multiplicity for most central collisions with mean impact parameter $\langle b \rangle = 2.4$ fm for RHIC and $\langle b \rangle = 2.65$ fm for LHC energy as shown in Fig. 2. Notice that the initial settings ($\tau_0 = 0.4$ fm, $\varepsilon_0 = 55$ GeV) are used in [41] to fit charged multiplicity for Au+Au $\sqrt{s_{NN}} = 200$ GeV collisions in centrality class 0 – 6%, which is a cross check for the current calculation. We will get back to the τ_0 -dependence of the squeezing effect below in Sec. III.

τ_0 [fm]	0.2	0.4	0.6
ε_0 [GeV/fm ³] at RHIC	135.5	55.0	32.6
ε_0 [GeV/fm ³] at LHC	413.9	166.4	98.0

Table III: Maximum energy density for (3+1)D ideal hydrodynamics starting from different values of τ_0 to get the same charged multiplicity distribution for RHIC and LHC energy.

Quantities of Interest/Observables

Since in non-central collisions the pressure gradients are enhanced along the x direction (transverse direction in reaction plane) and suppressed along the y direction (perpendicular to reaction plane), the fireball expands faster along x for such events. Accordingly, the final charged hadrons from the collective expansion have larger transverse momentum along this direction. How the spatial eccentricity ϵ_x is transferred to the momentum anisotropy ϵ_p is described step-by-step in the hydrodynamic simulations. The quantities ϵ_x and ϵ_p are useful to quantify the effect of the squeezing force density on the anisotropic expansion. To be precise, ϵ_x and ϵ_p are defined as,

$$\epsilon_x = \frac{\langle \varepsilon \gamma (y^2 - x^2) \rangle}{\langle \varepsilon \gamma (y^2 + x^2) \rangle}, \quad (9)$$

$$\epsilon_p = \frac{\langle T^{xx} - T^{yy} \rangle}{\langle T^{xx} + T^{yy} \rangle}, \quad (10)$$

where $\langle \rangle$ is an average over the transverse plane, ε and γ are the energy density and Lorentz factor, respectively,

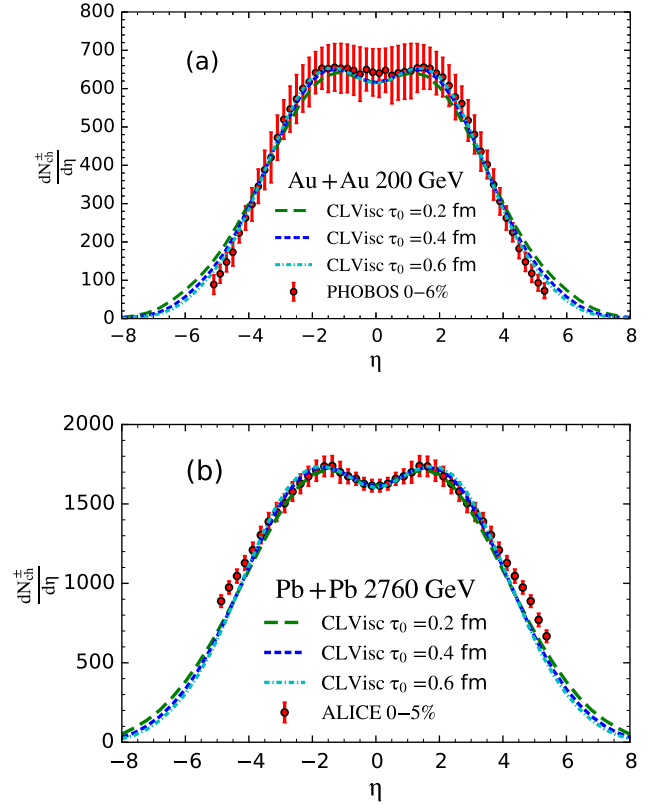


Figure 2: (color online) The charged multiplicity for (a) Au+Au $\sqrt{s_{NN}} = 200$ GeV collisions and (b) Pb+Pb $\sqrt{s_{NN}} = 2.76$ TeV collisions with 3 different groups of configurations for initial thermalization time τ_0 and maximum energy density ε_0 given in Table. III.

and T^{xx} and T^{yy} are the two diagonal components of the energy momentum tensor.

Another quantity that reflects the momentum anisotropy is the p_T differential elliptic flow v_2 of final charged hadrons at mid-rapidity, which is defined as,

$$v_2(p_T) \equiv \frac{\int d\phi \frac{dN}{dY dp_T d\phi} \cos(2(\phi - \Psi_2))}{\int d\phi \frac{dN}{dY dp_T d\phi}}. \quad (11)$$

Here, Ψ_2 is the event plane, which equals zero in the current study neglecting event-by-event fluctuations.

III. RESULTS

Pb+Pb $\sqrt{s_{NN}} = 2.76$ TeV collisions

Before performing full calculations, a simple comparison between the pressure gradients and the squeezing force density due to the magnetic field at thermalization time τ_0 is helpful to provide intuitive estimates. For the following results we set $\tau_0 = 0.2$ fm/c. The initial pressure gradients in the transverse plane (mid-rapidity) for

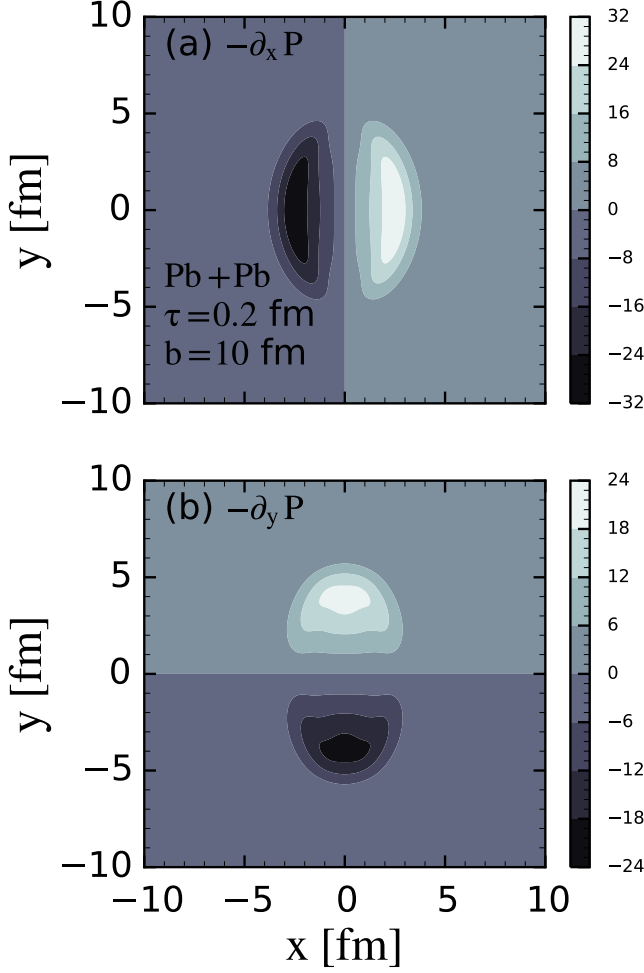


Figure 3: The pressure gradients for Pb+Pb $\sqrt{s_{NN}} = 2.76$ TeV collisions with impact parameter $b = 10$ fm.

Pb+Pb $\sqrt{s_{NN}} = 2.76$ TeV collisions with impact parameter $b = 10$ fm are shown in Fig. 3. As expected, the pressure gradient along the x direction exceeds that along the y direction, with a maximal value of around 32 GeV/fm⁴.

For a first calculation of the squeezing force density, we take the magnetic field profile of setting (E), which provides the highest initial magnetic field B_0 and the longest lifetime t_d . As Fig. 4 shows, the force density distribution³ is of similar shape and has magnitudes of about 10% compared to the pressure gradients. We also observe that the direction of the force density is roughly opposite to the pressure gradients – indeed providing a squeezing effect. For setting (E), where $2\sigma_x = \sigma_y = 2.6$ fm, the maximum squeezing force density is located at

³ Note that the local temperature given by the hydrodynamic simulation is employed in the susceptibility (5) to calculate the squeezing force density.

$x = \pm 1$ fm, while the maximum pressure gradient at $x = \pm 2$ fm. The region with high pressure gradients is more extended than the region, where the force density is pronounced. Thus it is also of interest to resize the high squeezing force density region by varying σ_x and σ_y , to investigate the effect on the anisotropic flow (setting (F)).

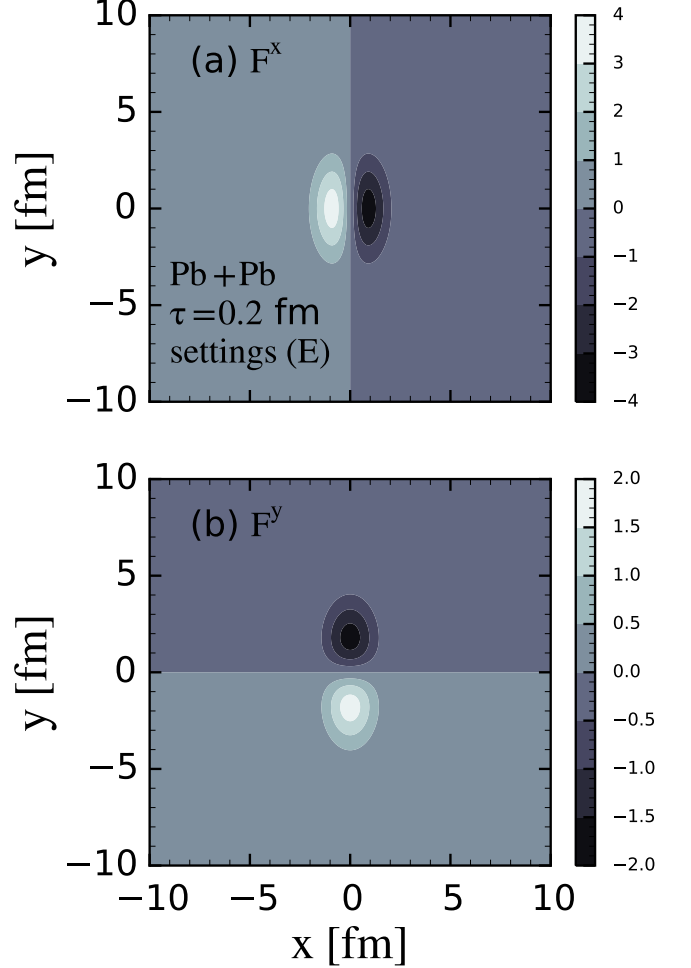


Figure 4: The squeezing force density (a) along the x direction and (b) along the y direction, for Pb+Pb $\sqrt{s_{NN}} = 2.76$ TeV collisions at $\tau_0 = 0.2$ fm, with the magnetic field given by setting (E).

Since the spatial distributions of both the squeezing force density and of the pressure gradients evolve with time, the previous comparison at $\tau = \tau_0$ clearly does not capture the full effect. To take into account the competition between the squeezing force density and the pressure gradients at each time step, we add the former as a source term for the energy-momentum tensor in the hydrodynamic equations, as in Eq. (3). In Fig. 5 we show the time evolution of the momentum anisotropy ϵ_p in the transverse plane for $B = 0$ and for settings (E), (G) and (F), cf. Tab. I. The squeezing force density with setting (E) reduces the momentum anisotropy by 5% at interme-

diate time, while that with larger σ_x and σ_y in setting (F) reduces ϵ_p by as much as 20%. Notice that the lifetime of the fireball in all cases increases, because the magnetic forces compress the system and, thus, reduce the rate of expansion.

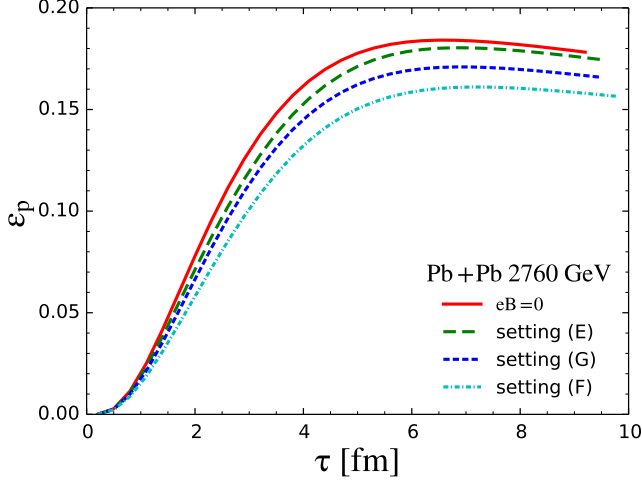


Figure 5: (color online) Time evolution of the momentum eccentricity ϵ_p for Pb+Pb $\sqrt{s_{NN}} = 2.76$ TeV collisions with impact parameter $b = 10$ fm, for (solid-line) $eB_0 = 0$, setting (E) (long-dashed line, $eB_0 = 1.33$ GeV 2 , $2\sigma_x = \sigma_y = 2.6$ fm), setting (G) (short-dashed line, $eB_0 = 1.0$ GeV 2 , $2\sigma_x = \sigma_y = 4.8$ fm) and setting (F) (dash-dotted line, $eB_0 = 1.33$ GeV 2 , $2\sigma_x = \sigma_y = 4.8$ fm).

The impact on the p_T differential anisotropic flow for direct π^+ emitted from the freezeout hypersurface, on the other hand, is less dramatic, as shown in Fig. 6. The squeezing force density with setting (E) reduces the elliptic flow by merely 1 – 2%. Increasing the spatial size of the magnetized region (setting (F)), the suppression of v_2 becomes around 6%. Both for ϵ_p and for v_2 , effects of similar size are observed for weaker but wide-spread magnetic fields, as given in setting (G) $eB_0 \approx 50 m_\pi^2$.

We also remark that besides B_0 , t_d and $\sigma_{x,y}$, a similarly relevant role is played by the thermalization time τ_0 . A lower τ_0 enhances the squeezing force in two ways. First, because the magnetic field is higher at earlier times and, thus, the gradient of \mathbf{B} is also increased. Second, because the temperature is also higher and the hot QGP is more prone to the squeezing effect due to its enhanced magnetic susceptibility, see Eq. (5). At the same time, the initial energy density and, thus, the pressure gradients are also very high for small τ_0 . The net dependence of the effect on τ_0 could thus be non-trivial.

In general, starting the hydrodynamic evolution at a larger value of τ_0 shifts the τ -dependence of ϵ_p to later times due to the zero initial transverse flow assumed in this study. However, as shown in Fig. 7, the elliptic flow on the freezeout hypersurface does not change considerably for three different values of τ_0 in the absence of mag-

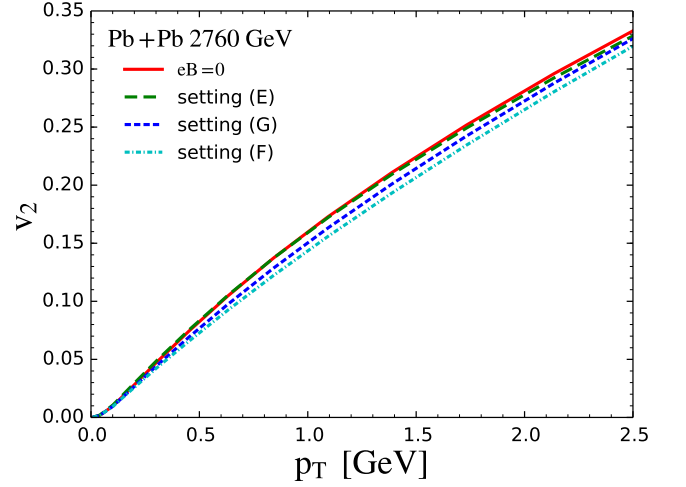


Figure 6: (color online) v_2 for direct π^+ at Pb+Pb $\sqrt{s_{NN}} = 2.76$ TeV collisions with impact parameter $b = 10$ fm, for (solid-line) $eB_0 = 0$, settings (E) (long-dashed line) $eB_0 = 1.33$ GeV 2 , $2\sigma_x = \sigma_y = 2.6$ fm, (G) (short-dashed line) $eB_0 = 1.0$ GeV 2 , $2\sigma_x = \sigma_y = 4.8$ fm and (F) (dash-dotted line) $eB_0 = 1.33$ GeV 2 , $2\sigma_x = \sigma_y = 4.8$ fm.

netic fields. For a long-lived magnetic field with $t_d \gg \tau_0$, the squeezing effect on v_2 is also insensitive to τ_0 . Note however, that this would not be the case for a magnetic field of shorter lifetime $t_d \approx \tau_0$. In the latter range of proper times, the exponential decay $B(\tau)$ suppresses the magnetic field – and, thus, the effect – considerably.

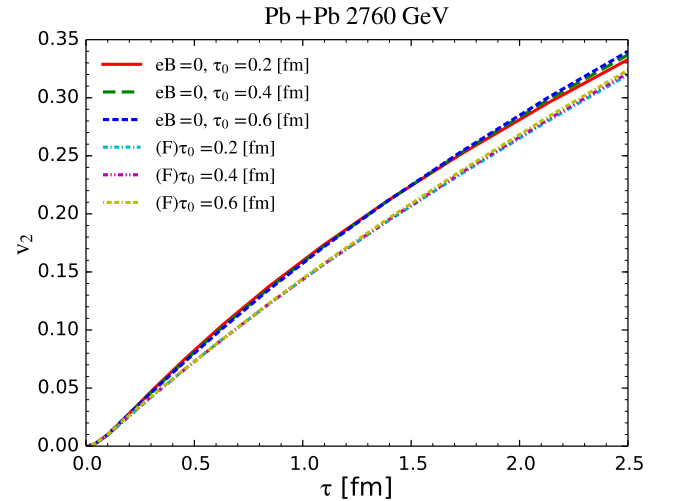


Figure 7: (color online) The effect of paramagnetic squeezing on the elliptic flow for $\tau_0 = 0.2, 0.4$ and 0.6 fm.

Au+Au $\sqrt{s_{NN}} = 200$ GeV collisions

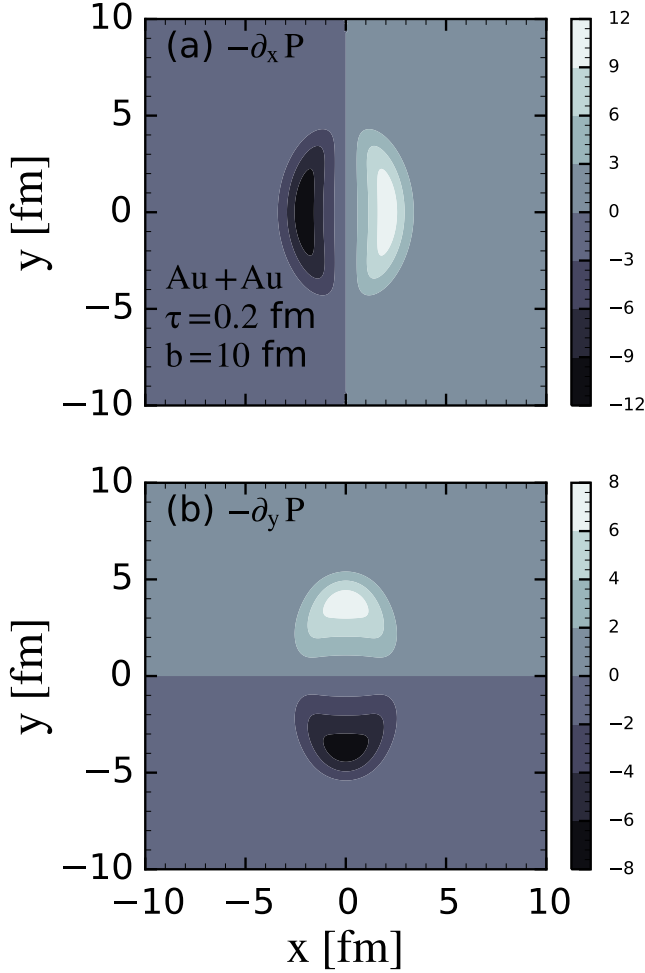


Figure 8: The pressure gradients for Au+Au $\sqrt{s_{NN}} = 200$ GeV collisions with impact parameter $b = 10$ fm.

Previous studies have shown that the magnetic field at RHIC energy decays much slower in the vacuum than at LHC energy due to the smaller relative speed between the colliding nuclei [35]. Here, we use a long-lived magnetic field with lifetime $t_d = 1.9$ fm at RHIC energy (setting (A)) to estimate the magnitude of the squeezing force density at $\tau_0 = 0.2$ fm. The maximum magnetic field at RHIC energy (0.09 GeV^2 used in this paper) is much smaller than that at LHC energy (1.33 GeV^2). The ratio of the maximal squeezing force density between RHIC and LHC collisions is thus proportional to $(0.09/1.33)^2 \approx 0.0046$. On the other hand, the maximal pressure gradients in the QGP at RHIC energy is around 1/3 of that at LHC energy, compare Fig. 8 to Fig. 3. The distribution of the squeezing force density for RHIC collisions is shown in Fig. 9, revealing that the paramagnetic squeezing is completely negligible at RHIC energy in the current framework.

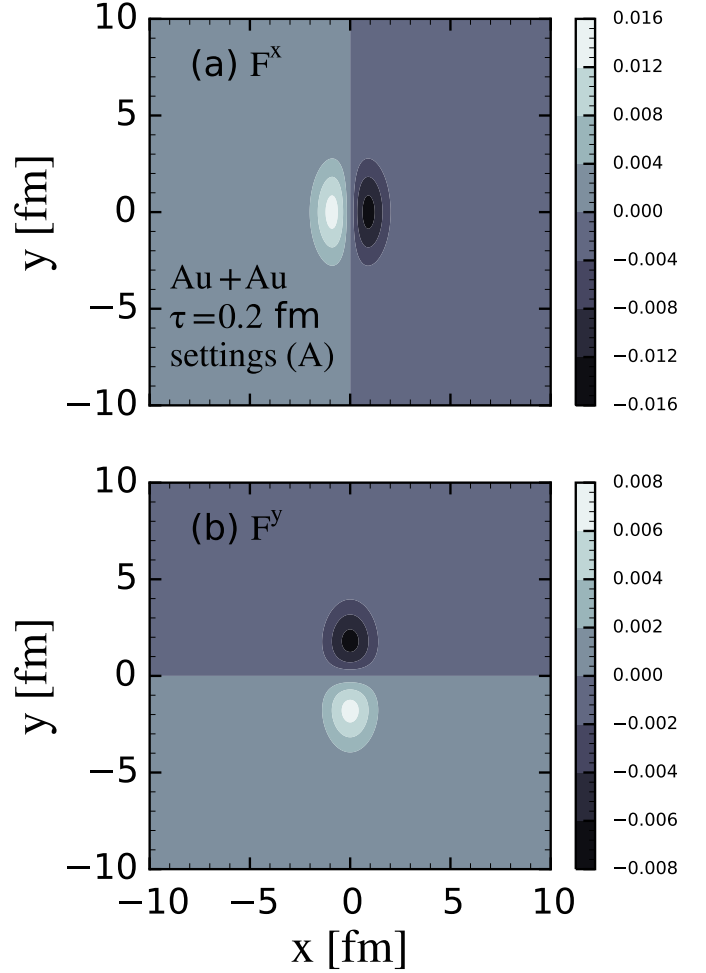


Figure 9: The squeezing force density for Au+Au $\sqrt{s_{NN}} = 200$ GeV collisions at $\tau_0 = 0.2$ fm, with the magnetic field given by setting (A).

IV. SUMMARY

We have studied the effect of paramagnetic squeezing [12] on the anisotropic expansion of bulk matter in non-central high-energy heavy-ion collisions, within a (3+1)-dimensional ideal hydrodynamic model. We found that the effect is sensitive to the space-time distribution of the magnetic field. A sizable effect is observed for long-lived and wide-spread magnetic fields at LHC energy. For such magnetic fields, the lifetime of the fireball (which is defined as the time interval between τ_0 and the complete freeze out when the temperature of all the fluid cells below T_{frz}) is elongated by $\sim 5\%$ as shown in Fig. 5, the momentum eccentricity averaged on the whole bulk matter reduces by 10 – 20%, while the anisotropic flow of π^+ from the freezeout hypersurface reduces by 6%. The slight reduction of v_2 due to the effect implies that the elliptic flow measured in the experiment is somewhat smaller than what would result from only the viscous

flow of the plasma. In other words, interpreting the experimental results for v_2 without taking the squeezing effect into account slightly overestimates the ratio η/s of the QGP. Strong suppression of momentum anisotropy ϵ_p also suggests that electromagnetic probes such as thermal photons and di-leptons might be more sensitive to the paramagnetic squeezing, since they are emitted from the whole QGP and HRG stage of the evolution and not just from the freezeout hypersurface. In addition, we also observed that the effect of the squeezing force density is negligible at RHIC energy, because the squeezing force density decreases much faster than the pressure gradients as the beam energy is reduced.

The current work can be extended in several ways. First, in real heavy-ion collisions, the initial charge density fluctuates strongly and the initial energy density is very lumpy. It is possible that the local magnetic field is large while the energy density is small [23]. The ratio between the squeezing force density and the pressure gradients for those regions can be very large and the effect for the anisotropic flow might be different. Second, the transport coefficients of the QGP are affected by strong magnetic fields: the shear viscosity η in the direction perpendicular to the magnetic field may be twice as small as in the direction of the field [10, 42, 43]. The ellip-

tic flow of final charged hadrons is predicted to be affected by this asymmetric shear viscosity over entropy density ratio η/s according to early studies in 2nd order viscous hydrodynamics [44, 45]. Relativistic magnetohydrodynamics with anisotropic shear viscosity needs to be developed for more accurate studies in the future.

Acknowledgments

We thank Andreas Schäfer for helpful discussions. LG. Pang and H. Petersen acknowledge funding of a Helmholtz Young Investigator Group VH-NG-822 from the Helmholtz Association and GSI. G. Endrődi acknowledges support from the DFG (Emmy Noether Programme EN 1064/2-1; and SFB/TRR 55). This work was supported in part by the Helmholtz International Center for the Facility for Antiproton and Ion Research (HIC for FAIR) within the framework of the Landes-Offensive zur Entwicklung Wissenschaftlich-Oekonomischer Exzellenz (LOEWE) program launched by the State of Hesse. Computational resources have been provided by the Center for Scientific Computing (CSC) at the Goethe-University of Frankfurt.

-
- [1] V. Skokov, A. Yu. Illarionov, and V. Toneev, *Int. J. Mod. Phys. A* **24**, 5925 (2009), 0907.1396.
 - [2] V. Voronyuk, V. D. Toneev, W. Cassing, E. L. Bratkovskaya, V. P. Konchakovski, and S. A. Voloshin, *Phys. Rev. C* **83**, 054911 (2011), 1103.4239.
 - [3] A. Bzdak and V. Skokov, *Phys. Lett. B* **710**, 171 (2012), 1111.1949.
 - [4] W.-T. Deng and X.-G. Huang, *Phys. Rev. C* **85**, 044907 (2012), 1201.5108.
 - [5] D. E. Kharzeev, K. Landsteiner, A. Schmitt, and H.-U. Yee, *Lect. Notes Phys.* **871**, 1 (2013), 1211.6245.
 - [6] D. E. Kharzeev, L. D. McLerran, and H. J. Warringa, *Nucl. Phys. A* **803**, 227 (2008), 0711.0950.
 - [7] K. Fukushima, D. E. Kharzeev, and H. J. Warringa, *Phys. Rev. D* **78**, 074033 (2008), 0808.3382.
 - [8] K. Tuchin, *Phys. Rev. C* **82**, 034904 (2010), [Erratum: *Phys. Rev. C* **83**, 039903 (2011)], 1006.3051.
 - [9] K. Tuchin, *Phys. Rev. C* **87**, 024912 (2013), 1206.0485.
 - [10] K. Tuchin, *Adv. High Energy Phys.* **2013**, 490495 (2013), 1301.0099.
 - [11] R. K. Mohapatra, P. S. Saumia, and A. M. Srivastava, *Mod. Phys. Lett. A* **26**, 2477 (2011), 1102.3819.
 - [12] G. S. Bali, F. Bruckmann, G. Endrődi, and A. Schäfer, *Phys. Rev. Lett.* **112**, 042301 (2014), 1311.2559.
 - [13] P. Elmfors, D. Persson, and B.-S. Skagerstam, *Phys. Rev. Lett.* **71**, 480 (1993), hep-th/9305004.
 - [14] G. Endrődi, *JHEP* **04**, 023 (2013), 1301.1307.
 - [15] G. S. Bali, F. Bruckmann, G. Endrődi, F. Gruber, and A. Schäfer, *JHEP* **04**, 130 (2013), 1303.1328.
 - [16] G. S. Bali, F. Bruckmann, G. Endrődi, and A. Schäfer, *PoS LATTICE2013*, 182 (2014), 1310.8145.
 - [17] C. Bonati, M. D'Elia, M. Mariti, F. Negro, and F. Sanfilippo, *Phys. Rev. Lett.* **111**, 182001 (2013), 1307.8063.
 - [18] C. Bonati, M. D'Elia, M. Mariti, F. Negro, and F. Sanfilippo, *Phys. Rev. D* **89**, 054506 (2014), 1310.8656.
 - [19] L. Levkova and C. DeTar, *Phys. Rev. Lett.* **112**, 012002 (2014), 1309.1142.
 - [20] G. S. Bali, F. Bruckmann, G. Endrődi, S. D. Katz, and A. Schäfer, *JHEP* **08**, 177 (2014), 1406.0269.
 - [21] L. Landau and E. Lifshitz, *Electrodynamics of Continuous Media* (1995).
 - [22] M. Lyutikov and S. Hadden, *Phys. Rev. E* **85**, 026401 (2012), 1112.0249.
 - [23] V. Roy, S. Pu, L. Rezzolla, and D. Rischke, *Phys. Lett. B* **750**, 45 (2015), 1506.06620.
 - [24] V. Roy and S. Pu, *Phys. Rev. C* **92**, 064902 (2015), 1508.03761.
 - [25] S. Pu, V. Roy, L. Rezzolla, and D. H. Rischke (2016), 1602.04953.
 - [26] S. Pu and D.-L. Yang (2016), 1602.04954.
 - [27] L. Pang, Q. Wang, and X.-N. Wang, *Phys. Rev. C* **86**, 024911 (2012), 1205.5019.
 - [28] L.-G. Pang, Y. Hatta, X.-N. Wang, and B.-W. Xiao, *Phys. Rev. D* **91**, 074027 (2015), 1411.7767.
 - [29] B. U. Felderhof and H. J. Kroh, *The Journal of Chemical Physics* **110** (1999).
 - [30] S. Borsányi, Z. Fodor, C. Hoelbling, S. D. Katz, S. Krieg, and K. K. Szabó, *Phys. Lett. B* **730**, 99 (2014), 1309.5258.
 - [31] L. McLerran and V. Skokov, *Nucl. Phys. A* **929**, 184 (2014), 1305.0774.
 - [32] H. Li, X.-l. Sheng, and Q. Wang (2016), 1602.02223.
 - [33] J. S. Schwinger, *Phys. Rev.* **82**, 664 (1951).
 - [34] K. Tuchin, *Phys. Rev. C* **88**, 024911 (2013), 1305.5806.
 - [35] Y. Zhong, C.-B. Yang, X. Cai, and S.-Q. Feng, *Chin.*

- Phys. **C39**, 104105 (2015), 1410.6349.
- [36] U. Gursoy, D. Kharzeev, and K. Rajagopal, Phys. Rev. **C89**, 054905 (2014), 1401.3805.
 - [37] B. G. Zakharov, Phys. Lett. **B737**, 262 (2014), 1404.5047.
 - [38] S. Gupta, Phys. Lett. **B597**, 57 (2004), hep-lat/0301006.
 - [39] S.-x. Qin, Phys. Lett. **B742**, 358 (2015), 1307.4587.
 - [40] M. Greif, I. Bouras, C. Greiner, and Z. Xu, Phys. Rev. **D90**, 094014 (2014), 1408.7049.
 - [41] B. Schenke, S. Jeon, and C. Gale, Phys. Rev. **C82**, 014903 (2010), 1004.1408.
 - [42] K. Tuchin, J. Phys. **G39**, 025010 (2012), 1108.4394.
 - [43] R. Critelli, S. I. Finazzo, M. Zaniboni, and J. Noronha, Phys. Rev. **D90**, 066006 (2014), 1406.6019.
 - [44] P. Romatschke and U. Romatschke, Phys. Rev. Lett. **99**, 172301 (2007), 0706.1522.
 - [45] H. Song and U. W. Heinz, Phys. Lett. **B658**, 279 (2008), 0709.0742.